Letter | Editors' Suggestion

Tunable cooperativity in coupled spin-cavity systems

Lukas Liensberger,[1,2,*] Franz X. Haslbeck,[3,4,†] Andreas Bauer,[3,5] Helmuth Berger,[6] Rudolf Gross,[1,2,7] Hans Huebl,[1,2,7] Christian Pfleiderer,[3,5,7] and Mathias Weiler[1,2,8,‡]

[1]*Walther-Meißner-Institut, Bayerische Akademie der Wissenschaften, 85748 Garching, Germany*
[2]*Physik-Department, Technische Universität München, 85748 Garching, Germany*
[3]*Lehrstuhl für Topologie korrelierter Systeme, Physik-Department, Technische Universität München, 85748 Garching, Germany*
[4]*Institute for Advanced Study, Technische Universität München, 85748 Garching, Germany*
[5]*Zentrum für QuantumEngineering (ZQE), Technische Universität München, D-85748 Garching, Germany*
[6]*Institut de Physique de la Matière Complexe, École Polytechnique Fédérale de Lausanne, 1015 Lausanne, Switzerland*
[7]*Munich Center for Quantum Science and Technology (MCQST), 80799 Munich, Germany*
[8]*Fachbereich Physik and Landesforschungszentrum OPTIMAS, Technische Universität Kaiserslautern, 67663 Kaiserslautern, Germany*

(Received 23 February 2021; revised 1 September 2021; accepted 2 September 2021; published 22 September 2021)

We experimentally study the tunability of the cooperativity in coupled spin-cavity systems by changing the magnetic state of the spin system via an external control parameter. As a model system, we use the skyrmion host material Cu_2OSeO_3 coupled to a microwave cavity resonator. We measure a dispersive coupling between the resonator and magnon modes in different magnetic phases of the material and model our results by using the input-output formalism. Our results show a strong tunability of the normalized coupling rate by magnetic field, allowing us to change the magnon-photon cooperativity from 1 to 60 at the phase boundaries of the skyrmion lattice state.

DOI: 10.1103/PhysRevB.104.L100415

Coupled magnon-photon systems become particularly interesting when the magnitude of the effective coupling rate g_{eff} between the magnons and photons in a microwave resonator exceeds their respective loss rates κ_{mag} and κ_{res}. In this limit, a coherent exchange of the quantized excitations is established [1,2] and for instance has been extensively studied for magnon-photon coupling in ferromagnets and ferrimagnets [3–7]. A measure of the coherent exchange of excitations in spin-cavity systems is the cooperativity. The possibility to tune the cooperativity by tiny changes of an external control parameter is a promising tool for applications. A possible route towards large tunability is offered by inducing changes in the spin system. To experimentally demonstrate this concept, we studied the skyrmion host material Cu_2OSeO_3, featuring several magnetic phases in a small magnetic field and temperature window.

Skyrmions are topologically stabilized spin solitons [8–18] exhibiting a rich spectrum of collective excitations of the spin system known as magnons. Theses excitations have been extensively studied in the limit of weak coupling to microwave circuits [19–25]. For potential applications such as realizing a novel magnetic state storage [26], it is necessary to couple the magnons to other quantized excitations such as photons [27] or (quasi)particles. While the coupling of the higher-order helimagnon modes [23] to an X-band (9.8 GHz) photonic resonator has been demonstrated [28], the magnon-photon coupling in the skyrmion lattice phase and the associated potential for tunable cooperativity remains an open issue so far.

In this Letter, we report the coupling of uniform-mode excitations of the insulating chiral magnet Cu_2OSeO_3 to microwave photons in a three-dimensional microwave cavity with a resonance frequency of 683.1 MHz. In contrast to earlier experiments [28], the magnon-photon coupling was addressed in all magnetic phases, including the skyrmion lattice phase. We find a large coupling rate of the breathing-mode skyrmion excitation to the cavity photons resulting in a high cooperativity $C = g_{\mathrm{eff}}^2/(\kappa_{\mathrm{mag}}\,\kappa_{\mathrm{res}}) > 50$. The cooperativity can be tuned by more than one order of magnitude by changing the external magnetic field magnitude by only $\sim$10 mT.

Cu_2OSeO_3 possesses a noncentrosymmetric cubic crystal structure with space group $P2_13$ [12,16] and exhibits a rich magnetic phase diagram [18] as schematically depicted in Fig. 1(a). Below the critical temperature $T_c \approx 58$ K, the long-range ordered helical, conical, and skyrmion phases form. At large magnetic fields, the system is in the field-polarized state. Above the transition temperature T_c, the system is paramagnetic. The phase diagram shown in Fig. 1(a) for $\boldsymbol{H}_0 \parallel [100]$ is representative for different crystallographic directions due to the rather weak magnetocrystalline anisotropy. In this study, the investigation of magnon-photon coupling was performed at $T = 56.5$ K as indicated by the dashed blue line in Fig. 1(a).

The different magnetic phases also differ in their magnetization dynamics [16,19,21]. Figure 1(b) shows the typical spectrum of resonance frequencies of the uniform fundamental modes of an insulating chiral magnet as a function of the

*Lukas.Liensberger@wmi.badw.de
†Present address: Walther-Meißner-Institut, Bayerische Akademie der Wissenschaften, 85748 Garching, Germany.
‡weiler@physik.uni-kl.de

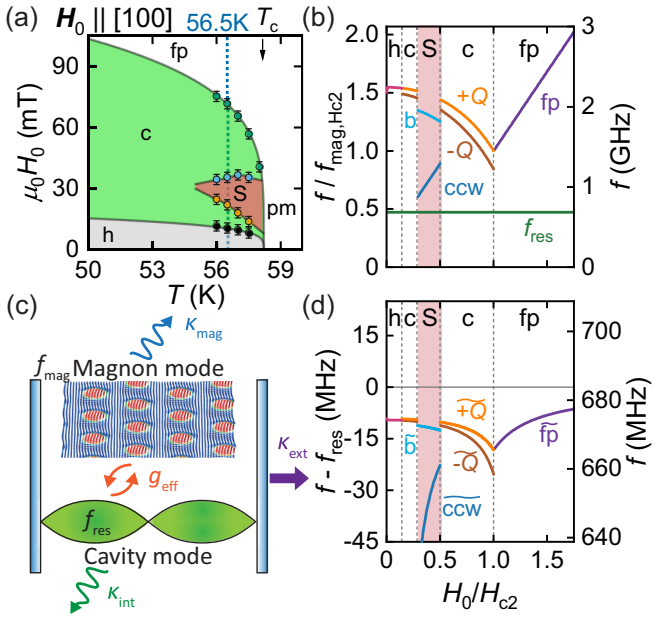

FIG. 1. Microwave dynamics in Cu_2OSeO_3. (a) Magnetic phase diagram extracted from broadband magnetic resonance measurements. The following magnetic phases are distinguished: field-polarized (fp), conical (c), helical (h) phase, skyrmion lattice phase (S), paramagnetic (pm) phase. Note that the crossover between the fp and the pm regime above T_c is not resolved. (b) Schematic magnetic field dependence of the uncoupled, uniform resonance frequencies of the magnon modes f_{mag} in a chiral magnet. The resonance frequency of the resonator f_{res} is lower than all magnon frequencies. Normalized and absolute frequencies are shown on the left and right ordinate, respectively. (c) Illustration of the input-output formalism and the parameters of Eq. (1). The following parameters are established: magnon resonance frequency f_{mag}, magnon loss rate κ_{mag}, cavity resonance frequency f_{res}, cavity internal κ_{int} and external loss rate κ_{ext}, and effective coupling rate g_{eff}. (d) Frequency shift of the resonator mode in a coupled magnon-photon system calculated using the input-output formalism with a constant coupling rate $g_{eff}/(2\pi) = 120$ MHz in all magnetic phases. The hybridized magnon-cavity modes are denoted by tildes.

external magnetic field. Starting at large fields, in the field-polarized phase (fp) only one resonance mode is observed. Here, all the magnetic moments precess in phase (ferrimagnetic resonance). By decreasing the magnetic field, the system enters the conical phase (c), where, depending on the details of the demagnetization, the $\pm Q$ modes are observed [21]. In the skyrmion phase (S), the breathing mode (b), the counterclockwise (ccw) and the clockwise mode can couple to a uniform driving field [29]. The clockwise mode is omitted due to its comparably small spectral weight. For a more detailed characterization of these modes in chiral magnets, we refer to Ref. [21].

To model the dynamics of the coupled chiral magnet-cavity system we employ the input-output formalism [3,30–33]. A schematic of the physical mechanisms underlying the coupling and its description is shown in Fig. 1(c). The photons in a microwave resonator with frequency f_{res} can interact with the magnons of the chiral magnet with frequency f_{mag} (via the dipolar interaction) with an effective coupling strength g_{eff}.

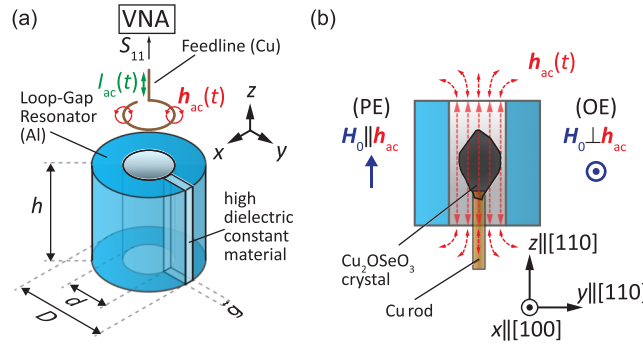

FIG. 2. Experimental setup. (a) Schematic of the loop-gap resonator and feedline design. (b) Side view of the resonator and the Cu_2OSeO_3 crystal mounted on a copper rod and placed inside the cavity. Note the different configurations of static external magnetic field $\boldsymbol{H}_0$ relative to the oscillating magnetic field $\boldsymbol{h}_{ac}$.

The cavity photons and the magnons in Cu_2OSeO_3 possess certain lifetimes and thus decay with loss rates κ_{res} and κ_{mag}, respectively. Note that the total cavity loss rate κ_{res} is given by the sum of the internal loss rate κ_{int} and the external loss rate κ_{ext} of the cavity. The latter quantifies the coupling strength of the cavity to the feedline. For the measured S_{11} parameter of the vector network analyzer (VNA) the input-output formalism yields [4,28,30,31,33]

$$S_{11}(f) = -1 + \frac{2\kappa_{ext}}{\imath \cdot 2\pi (f_{res} - f) + \kappa_{res} + \frac{g_{eff}^2}{\imath \cdot 2\pi (f_{mag} - f) + \kappa_{mag}}}, \tag{1}$$

with $\kappa_{res} = \kappa_{int} + \kappa_{ext}$. The resonance frequency of the cavity, $f_{res} = 683.8$ MHz at 56.5 K is lower than all resonance frequencies of the magnon modes, as shown by our broadband magnetic resonance spectroscopy in the Supplemental Material [34]. This significant detuning of the two systems restricts our analysis to the dispersive limit [28]. The input-output formalism remains valid for $f_{res} \neq f_{mag}$ [28]. Using the resonance frequencies f_{mag} and f_{res} shown in Fig. 1(b) and $g_{eff}/(2\pi) = 120$ MHz (comparable to the value determined below), we calculate the modified resonance frequencies of the coupled magnon-cavity system close to 680 MHz by minimizing $|S_{11}(f)|$ given by Eq. (1) for each magnetic field H_0. The result is shown in Fig. 1(d). In all magnetic phases of Cu_2OSeO_3, the frequency of the hybridized magnon-photon mode is reduced to values well below the resonance frequency f_{res} of the unperturbed cavity due to the formation of normal modes.

To verify the expected magnon-photon coupling we used the measurement setup schematically depicted in Fig. 2(a). We fabricated a loop-gap resonator [35] based on an aluminum cylinder (height $h = 22$ mm, inner diameter $d = 10$ mm, outer diameter $D = 22$ mm). The gap with a width of $g = 0.7$ mm is filled with a high-dielectric-constant material. A copper loop was connected to the center conductor of a subminiature version A (SMA) connector to inductively couple the microwave to the resonator. The feedline was connected to a VNA and the complex reflection parameter S_{11} was measured as a function of the microwave frequency f

and the external magnetic field $\boldsymbol{H}_0$. The applied microwave power was 0 dBm, and we confirmed that the magnetization dynamics of the system is in the linear regime. The geometry and placement of the coupling loop was adjusted to maximize the microwave power absorbed by the cavity.

The Cu_2OSeO_3 single crystal was mounted on a copper rod which is inserted roughly 6 mm into the cavity, so that the single crystal is in the center of the resonator (for details, see Supplemental Material [34] Fig. S1). The loaded quality factor of the cavity was 350(26) at a resonance frequency $f_{\mathrm{res}} = 683.8$ MHz. The cavity with the sample was placed into a helium-flow cryostat equipped with a three-dimensional (3D) vector magnet. We slowly sweep the external magnetic field $\boldsymbol{H}_0$ keeping the system in equilibrium at each value of H_0. The resonator features a clearly defined direction of the oscillating driving field $\boldsymbol{h}_{\mathrm{ac}}$ with good homogeneity inside the cavity as depicted in Fig. 2(b) and confirmed by our finite-element modeling (see Figs. S3 and S4 [34]). Therefore, it is possible to investigate configurations with $\boldsymbol{H}_0 \parallel \boldsymbol{h}_{\mathrm{ac}}$ and $\boldsymbol{H}_0 \perp \boldsymbol{h}_{\mathrm{ac}}$ as indicated in Fig. 2(b). We will refer to the situation $\boldsymbol{H}_0 \parallel [110] \parallel \boldsymbol{h}_{\mathrm{ac}}$ as parallel excitation (PE) and to $\boldsymbol{H}_0 \parallel [100] \perp \boldsymbol{h}_{\mathrm{ac}}$ as orthogonal excitation (OE).

The skyrmion lattice forms a periodic hexagonal lattice perpendicular to the external magnetic field [8]. Its breathing mode is dominantly excited in the PE configuration, while the counterclockwise mode is dominantly excited in the OE configuration [16,19] as depicted in Fig. 3(a). All further dynamical modes are also expected to dominantly couple in the OE configuration.

Typical results from the reflection measurements performed with the VNA are shown in Fig. 3(b) in the form of the background-corrected (see Fig. S5 [34]) reflection parameter $|S_{11}|$. In order to account for different demagnetization fields, the magnetic field is normalized to the critical field $H_{c2} = 71.7$ mT for OE and 39.1 mT for PE. For OE, a shift of the cavity resonance frequency is observed in the field-polarized and conical phase, in agreement with Fig. 1(d). In the skyrmion lattice phase, we observe coupling between the ccw mode and the cavity photons. There is no distinct transition from the conical to the helical phase because the external magnetic field $\boldsymbol{H}_0$ is applied along the magnetic easy axis of the cubic anisotropy in Cu_2OSeO_3 [36]. Thus the system does not form domains upon decreasing field but keeps a small net moment along $\boldsymbol{H}_0$ [37–39].

If the static magnetic field is parallel to the oscillating driving field (PE), no coupling is observed in the field-polarized and conical phases. As the magnetic moments are aligned with $\boldsymbol{H}_0$, the driving field $\boldsymbol{h}_{\mathrm{ac}}$ cannot exert a torque on the precessing magnetic moments. In the skyrmion lattice phase, we clearly observe coupled dynamics of the cavity and the breathing mode of the Cu_2OSeO_3 spin system. This coupling is most efficient for the driving field $\boldsymbol{h}_{\mathrm{ac}}$ parallel to the static field $\boldsymbol{H}_0$ [see Fig. 3(a)]. In the helical phase, a finite coupling is observed in contrast to the OE case. The domain population in the helical phase crucially depends on the field direction as well as on the temperature and field history. For decreasing magnetic field along the ⟨110⟩ direction, two domains are equally populated, leading to a finite angle between them [37–39]. Consequently, a finite coupling in the helical phase is observed.

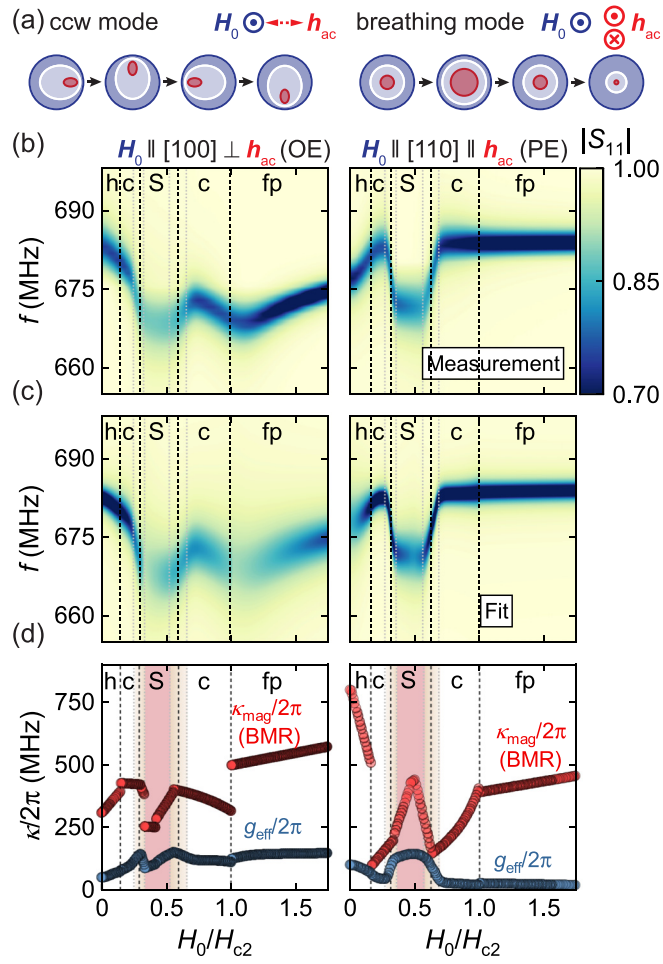

FIG. 3. Magnon-photon coupling in a skyrmion host material. (a) Illustration of the two dominant skyrmion resonance modes. The blue and red color correspond to the local magnetization pointing parallel and antiparallel to $\boldsymbol{H}_0$, respectively, and the gray color to noncollinear to $\boldsymbol{H}_0$. The oscillating driving field $\boldsymbol{h}_{\mathrm{ac}}$ is either orthogonal (ccw mode) or parallel (breathing mode) to the external magnetic field $\boldsymbol{H}_0$. (b) Measured reflection parameter $|S_{11}|$ as a function of the magnetic field H_0 and the applied microwave frequency f. The vertical dashed lines indicate phase boundaries (cf. Fig. S6 [34]). The magnetic fields are normalized to the critical field H_{c2}. (c) Simulated spectrum calculated with Eq. (1). (d) Coupling rate g_{eff} extracted from fitting Eq. (1) to frequency traces at fixed magnetic field and magnon loss rate κ_{mag} from broadband magnetic resonance (BMR) measurements (cf. Fig. S8 [34]) used to calculate the spectrum shown in (c). The fit error bars are smaller than the symbol size. The rather broad phase transition S ↔ c due to the irregular shape of the single crystal is indicated by the orange shading around the dashed gray lines.

We now turn to a quantitative evaluation of the magnon-photon coupling by employing the input-output formalism in the following three steps: First, we extract the external loss rate κ_{ext}, the total loss rate κ_{res}, and resonance frequency f_{res} of the cavity by fitting Eq. (1) to a frequency trace of the reflection parameter $|S_{11}|$ at the largest static magnetic field available ($\mu_0 H_0 = 126$ mT for PE). The system is assumed to be unperturbed and therefore we set $g_{\mathrm{eff}} = 0$. The following values are inferred: $f_{\mathrm{res}} = 683.8$ MHz, $\kappa_{\mathrm{res}}/(2\pi) =$

1.041(4) MHz, and $\kappa_{ext}/(2\pi) = 0.424(2)$ MHz. The internal loss rate of the cavity κ_{int} is larger than the external loss rate κ_{ext}, indicating that the cavity is slightly undercoupled [40].

In a second step, we keep these parameters fixed and fit Eq. (1) to all frequency traces of $|S_{11}|$ for a series of external magnetic fields H_0 along both magnetic field directions. From these fits, the coupling strength g_{eff} is extracted for each H_0. The field-dependent resonance frequency of the different magnon modes f_{mag} and the magnon decay rate κ_{mag} are taken from broadband magnetic resonance spectroscopy data measured using the same crystal (see Figs. S7 and S8 [34]). Note that the cavity-based technique probes the whole sample volume while the broadband technique is only sensitive to spin dynamics within the first few μm of the sample above the coplanar waveguide. Due to the irregular shape of the crystal, its demagnetization fields are inhomogeneous, which leads to minor deviations in the resonance frequencies and loss rates of the magnon modes and magnetic fields of the phase transition compared to the broadband magnetic resonance technique.

Using the extracted parameters, we recalculate $|S_{11}|$ using Eq. (1) with results displayed in Fig. 3(c). Good agreement between this fit and the measurement in Fig. 3(b) is found. The obtained parameters κ_{mag} and g_{eff} are shown in Fig. 3(d). The magnon decay rate κ_{mag} is larger than the coupling strength g_{eff} in all magnetic phases, which classifies the system to be in the Purcell coupling regime with $\kappa_{res} < g_{eff} < \kappa_{mag}$ [4]. For PE, the coupling strength outside the skyrmion lattice and helical phase becomes small. In the skyrmion lattice phase, the breathing mode couples to the cavity and we extract almost the same effective coupling rate g_{eff} as for the counterclockwise rotation mode. Note that the resonator properties may subtly evolve with magnetic field, also leading to minor changes in g_{eff}.

In the field-polarized phase, we estimate the expected coupling strength as $g_{eff}/(2\pi) = g_J\mu_B/(2h)\sqrt{\mu_0 h f_{res}(N/V)(\eta/2)}$ [3] with $g_J \approx 2$, the Bohr magneton μ_B, and the Planck constant h. The volume of the crystal $V \approx 1.0 \times 10^{-7}$ m^3 yields a total effective spin number $N \approx 5.6 \times 10^{20}$ [28] and the filling factor $\eta = V/V_{res} \approx 0.058$ with the mode volume of the resonator field mode $V_{res} = (d/2)^2\pi h = 1.7 \times 10^{-6}$ m^3. With these values, we expect a coupling strength of $g_{eff}/(2\pi) \approx 134$ MHz, which is in good agreement with the extracted value in the fp phase for the OE configuration in Fig. 3(d).

In the third and final step, the cooperativity C of the system is calculated as a measure for the coherent exchange of excitations. The cooperativity defined as [3,4,41,42]

$$C = \frac{g_{eff}^2}{\kappa_{res} \cdot \kappa_{mag}} \tag{2}$$

is shown in Fig. 4. For OE, the cooperativity increases from $C \approx 8$ in the helical phase to $C \approx 50$ in the skyrmion lattice phase. Similar values for the cooperativity are found in the skyrmion lattice, conical, and field-polarized phases away from the phase-transition regions.

For PE, the cooperativity C is small or close to unity in the field-polarized and conical phase. A drastic change of the cooperativity is observed when the magnetic phase transition

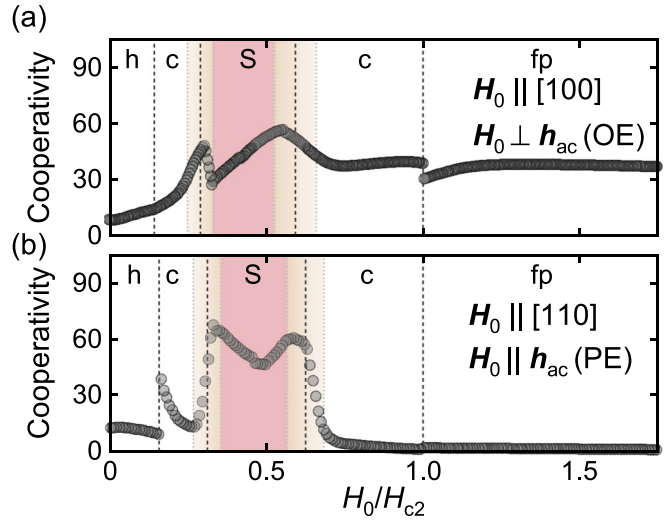

FIG. 4. Cooperativity calculated by using Eq. (2) and the parameters shown in Fig. 3(d). (a) Orthogonal excitation (OE). (b) Parallel excitation (PE), for which the cooperativity can be tuned from 1 to 60. The fit error bars are smaller than the symbol size.

into the skyrmion lattice phase is induced by a small variation of the magnetic field. The cooperativity reaches a maximum value of $C \approx 60$ and can be tuned between its maximum and minimum value by changing the external magnetic field by $\sim$10 mT. Here, we utilize that the breathing mode exhibits a different excitation geometry compared to the magnon excitations in the other magnetic phases. This property is unique to the topologically protected skyrmion lattice phase. At the phase boundaries, the magnon-photon cooperativity distinctly changes with magnetic field due to the induced phase transition. This allows us to control the effective coupling rate g_{eff} between the microwave photons and the magnons in Cu_2OSeO_3. At the boundary of the helical phase, the helices reorient with decreasing magnetic field and gain components orthogonal to $\boldsymbol{h}_{ac}$. Thus the microwave photons can couple to the spin system more efficiently. However, such transitions lack the pronounced excitation selectivity.

In conclusion, we experimentally demonstrated a selective coupling between magnetic excitations in the chiral magnet Cu_2OSeO_3 and photons inside a three-dimensional microwave cavity by using magnetic resonance spectroscopy. The coupling between the dynamics of topologically protected skyrmions and the photons in the cavity is mediated by the dipolar interaction and a high magnon-photon cooperativity is observed. By changing the magnetic field in a small field range, the system undergoes a phase transition resulting in a strong tunability of the magnon-photon coupling rate and therefore the magnon-photon cooperativity. Such phase transitions can also be induced by other control parameters including temperature, or electric field [43–45]. For suitably polarized microwave photons, we observe a high contrast in the photon-magnon cooperativity between regimes with the skyrmion breathing mode and topologically trivial spin dynamics. This may allow the sensitive detection of skyrmion dynamics in technologically relevant materials used for magnetic racetrack applications [14]. The tunable cooperativity close to the skyrmion phase transition may be exploited in

hybrid magnon-qubit systems [1,46] that are so far based on yttrium iron garnet, where the tuning mechanism described here is not available. As a next step in this direction, tunable photon coupling to spin dynamics in the low-temperature skyrmion phase of Cu_2OSeO_3 [25,47,48] could be explored.

Note added. Recently, we became aware of a related study showing the coupling of microwave photons to the topological spin texture in Cu_2OSeO_3 [49].

We thank A. Habel for technical support. This work has been funded by the Deutsche Forschungsgemeinschaft (DFG, German Research Foundation) via the excellence cluster MCQST under Germany's Excellence Strategy EXC-2111 (Project No. 390814868). L.L. and M.W. gratefully acknowledge the financial support of the DFG via the Projects No. WE 5386/4-1 and No. WE 5386/5-1 (SPP2137 Skyrmionics). F.X.H., A.B., and C.P. acknowledge financial support from the DFG under TRR80 (From Electronic Correlations to Functionality, Project No. 107745057, Projects E1 and F7) and SPP2137 (Skyrmionics, Project No. 403191981, Grant No. PF393/19), and from the European Research Council (ERC) through Advanced Grants No. 291079 (TOPFIT) and No. 788031 (ExQuiSid). The work by F.X.H. was supported through a Hans Fischer fellowship of the Technische Universität München-Institute for Advanced Study for Marc Janoschek, funded by the German Excellence Initiative and the European Union Seventh Framework Programme under Grant Agreement No. 291763.

[1] D. Lachance-Quirion, Y. Tabuchi, A. Gloppe, K. Usami, and Y. Nakamura, Hybrid quantum systems based on magnonics, Appl. Phys. Express **12**, 070101 (2019).

[2] A. Frisk Kockum, A. Miranowicz, S. De Liberato, S. Savasta, and F. Nori, Ultrastrong coupling between light and matter, Nat. Rev. Phys. **1**, 19 (2019).

[3] H. Huebl, C. W. Zollitsch, J. Lotze, F. Hocke, M. Greifenstein, A. Marx, R. Gross, and S. T. B. Goennenwein, High Cooperativity in Coupled Microwave Resonator Ferrimagnetic Insulator Hybrids, Phys. Rev. Lett. **111**, 127003 (2013).

[4] X. Zhang, C. L. Zou, L. Jiang, and H. X. Tang, Strongly Coupled Magnons and Cavity Microwave Photons, Phys. Rev. Lett. **113**, 156401 (2014).

[5] L. Bai, M. Harder, Y. P. Chen, X. Fan, J. Q. Xiao, and C.-M. Hu, Spin Pumping in Electrodynamically Coupled Magnon-Photon Systems, Phys. Rev. Lett. **114**, 227201 (2015).

[6] T. Liu, X. Zhang, H. X. Tang, and M. E. Flatté, Optomagnonics in magnetic solids, Phys. Rev. B **94**, 060405(R) (2016).

[7] M. Harder and C.-M. Hu, Cavity Spintronics: An early review of recent progress in the study of magnon-photon level repulsion, in *Solid State Physics*, edited by R. E. Camley and R. L. Stamps (Academic, Cambridge, MA, 2018), Vol. 69, pp. 47–121.

[8] S. Mühlbauer, B. Binz, F. Jonietz, C. Pfleiderer, A. Rosch, A. Neubauer, R. Georgii, and P. Boni, Skyrmion lattice in a chiral magnet, Science **323**, 915 (2009).

[9] F. Jonietz, S. Mühlbauer, C. Pfleiderer, A. Neubauer, W. Munzer, A. Bauer, T. Adams, R. Georgii, P. Boni, R. A. Duine, K. Everschor, M. Garst, and A. Rosch, Spin transfer torques in MnSi at ultralow current densities, Science **330**, 1648 (2010).

[10] T. Adams, A. Chacon, M. Wagner, A. Bauer, G. Brandl, B. Pedersen, H. Berger, P. Lemmens, and C. Pfleiderer, Long-Wavelength Helimagnetic Order and Skyrmion Lattice Phase in Cu_2OSeO_3, Phys. Rev. Lett. **108**, 237204 (2012).

[11] T. Schulz, R. Ritz, A. Bauer, M. Halder, M. Wagner, C. Franz, C. Pfleiderer, K. Everschor, M. Garst, and A. Rosch, Emergent electrodynamics of skyrmions in a chiral magnet, Nat. Phys. **8**, 301 (2012).

[12] S. Seki, X. Z. Yu, S. Ishiwata, and Y. Tokura, Observation of skyrmions in a multiferroic material, Science **336**, 198 (2012).

[13] X. Yu, N. Kanazawa, W. Zhang, T. Nagai, T. Hara, K. Kimoto, Y. Matsui, Y. Onose, and Y. Tokura, Skyrmion flow near room temperature in an ultralow current density, Nat. Commun. **3**, 988 (2012).

[14] A. Fert, V. Cros, and J. Sampaio, Skyrmions on the track, Nat. Nanotechnol. **8**, 152 (2013).

[15] N. Nagaosa and Y. Tokura, Topological properties and dynamics of magnetic skyrmions, Nat. Nanotechnol. **8**, 899 (2013).

[16] M. Garst, J. Waizner, and D. Grundler, Collective spin excitations of helices and magnetic skyrmions: Review and perspectives of magnonics in non-centrosymmetric magnets, J. Phys. D: Appl. Phys. **50**, 293002 (2017).

[17] N. Kanazawa, S. Seki, and Y. Tokura, Noncentrosymmetric magnets hosting magnetic skyrmions, Adv. Mater. **29**, 1603227 (2017).

[18] A. Bauer, A. Chacon, M. Halder, and C. Pfleiderer, Skyrmion lattices far from equilibrium, in *Topology in Magnetism*, edited by J. Zang, V. Cros, and A. Hoffmann, Springer Series in Solid-State Sciences Vol. 192 (Springer, Cham, 2018), Chap. 5, pp. 151–176.

[19] Y. Onose, Y. Okamura, S. Seki, S. Ishiwata, and Y. Tokura, Observation of Magnetic Excitations of Skyrmion Crystal in a Helimagnetic Insulator Cu_2OSeO_3, Phys. Rev. Lett. **109**, 037603 (2012).

[20] Y. Okamura, F. Kagawa, M. Mochizuki, M. Kubota, S. Seki, S. Ishiwata, M. Kawasaki, Y. Onose, and Y. Tokura, Microwave magnetoelectric effect via skyrmion resonance modes in a helimagnetic multiferroic, Nat. Commun. **4**, 2391 (2013).

[21] T. Schwarze, J. Waizner, M. Garst, A. Bauer, I. Stasinopoulos, H. Berger, C. Pfleiderer, and D. Grundler, Universal helimagnon and skyrmion excitations in metallic, semiconducting and insulating chiral magnets, Nat. Mater. **14**, 478 (2015).

[22] Y. Okamura, F. Kagawa, S. Seki, M. Kubota, M. Kawasaki, and Y. Tokura, Microwave Magnetochiral Dichroism in the Chiral-Lattice Magnet Cu_2OSeO_3, Phys. Rev. Lett. **114**, 197202 (2015).

[23] M. Weiler, A. Aqeel, M. Mostovoy, A. Leonov, S. Geprägs, R. Gross, H. Huebl, T. T. M. Palstra, and S. T. B. Goennenwein, Helimagnon Resonances in an Intrinsic Chiral Magnonic Crystal, Phys. Rev. Lett. **119**, 237204 (2017).

[24] I. Stasinopoulos, S. Weichselbaumer, A. Bauer, J. Waizner, H. Berger, S. Maendl, M. Garst, C. Pfleiderer, and D. Grundler,

Low spin wave damping in the insulating chiral magnet Cu_2OSeO_3, Appl. Phys. Lett. **111**, 032408 (2017).

[25] A. Aqeel, J. Sahliger, T. Taniguchi, S. Mändl, D. Mettus, H. Berger, A. Bauer, M. Garst, C. Pfleiderer, and C. H. Back, Microwave Spectroscopy of the Low-Temperature Skyrmion State in Cu_2OSeO_3, Phys. Rev. Lett. **126**, 017202 (2021).

[26] Y. Li, W. Zhang, V. Tyberkevych, W.-K. Kwok, A. Hoffmann, and V. Novosad, Hybrid magnonics: Physics, circuits, and applications for coherent information processing, J. Appl. Phys. **128**, 130902 (2020).

[27] Y. Tabuchi, S. Ishino, A. Noguchi, T. Ishikawa, R. Yamazaki, K. Usami, and Y. Nakamura, Coherent coupling between a ferromagnetic magnon and a superconducting qubit, Science **349**, 405 (2015).

[28] L. V. Abdurakhimov, S. Khan, N. A. Panjwani, J. D. Breeze, M. Mochizuki, S. Seki, Y. Tokura, J. J. L. Morton, and H. Kurebayashi, Magnon-photon coupling in the noncollinear magnetic insulator Cu_2OSeO_3, Phys. Rev. B **99**, 140401(R) (2019).

[29] M. Mochizuki, Spin-Wave Modes and Their Intense Excitation Effects in Skyrmion Crystals, Phys. Rev. Lett. **108**, 017601 (2012).

[30] D. F. Walls and G. J. Milburn, *Quantum Optics*, 2nd ed. (Springer, Berlin, 2008).

[31] A. A. Clerk, M. H. Devoret, S. M. Girvin, F. Marquardt, and R. J. Schoelkopf, Introduction to quantum noise, measurement, and amplification, Rev. Mod. Phys. **82**, 1155 (2010).

[32] D. I. Schuster, A. P. Sears, E. Ginossar, L. DiCarlo, L. Frunzio, J. J. L. Morton, H. Wu, G. A. D. Briggs, B. B. Buckley, D. D. Awschalom, and R. J. Schoelkopf, High-Cooperativity Coupling of Electron-Spin Ensembles to Superconducting Cavities, Phys. Rev. Lett. **105**, 140501 (2010).

[33] E. Abe, H. Wu, A. Ardavan, and J. J. L. Morton, Electron spin ensemble strongly coupled to a three-dimensional microwave cavity, Appl. Phys. Lett. **98**, 251108 (2011).

[34] See Supplemental Material at http://link.aps.org/supplemental/10.1103/PhysRevB.104.L100415 for details of the used Cu_2OSeO_3 crystal, loop-gap resonator including finite-element simulations, background subtraction of cavity magnetic resonance data, broadband magnetic resonance spectroscopy (BMR), extracted resonance frequencies, extracted magnon loss rates, and for additional measurement results of the spin-cavity system, which includes Refs. [50–54].

[35] G. A. Rinard and G. R. Eaton, Loop-gap resonators, in *Biomedical EPR, Part B: Methodology, Instrumentation, and Dynamics*, edited by S. R. Eaton, G. R. Eaton, and L. J. Berliner (Springer, Boston, 2005), Vol. 24/B, Chap. 2, pp. 19–52.

[36] M. Halder, A. Chacon, A. Bauer, W. Simeth, S. Mühlbauer, H. Berger, L. Heinen, M. Garst, A. Rosch, and C. Pfleiderer, Thermodynamic evidence of a second skyrmion lattice phase and tilted conical phase in Cu_2OSeO_3, Phys. Rev. B **98**, 144429 (2018).

[37] A. Bauer, A. Chacon, M. Wagner, M. Halder, R. Georgii, A. Rosch, C. Pfleiderer, and M. Garst, Symmetry breaking, slow relaxation dynamics, and topological defects at the field-induced helix reorientation in MnSi, Phys. Rev. B **95**, 024429 (2017).

[38] J. Kindervater, I. Stasinopoulos, A. Bauer, F. X. Haslbeck, F. Rucker, A. Chacon, S. Mühlbauer, C. Franz, M. Garst, D. Grundler, and C. Pfleiderer, Weak Crystallization of Fluctuating Skyrmion Textures in MnSi, Phys. Rev. X **9**, 041059 (2019).

[39] P. Milde, L. Köhler, E. Neuber, P. Ritzinger, M. Garst, A. Bauer, C. Pfleiderer, H. Berger, and L. M. Eng, Field-induced reorientation of helimagnetic order in Cu_2OSeO_3 probed by magnetic force microscopy, Phys. Rev. B **102**, 024426 (2020).

[40] N. J. Lambert, A. Rueda, F. Sedlmeir, and H. G. L. Schwefel, Coherent conversion between microwave and pptical photons—an overview of physical implementations, Adv. Quantum Technol. **3**, 1900077 (2020).

[41] P. F. Herskind, A. Dantan, J. P. Marler, M. Albert, and M. Drewsen, Realization of collective strong coupling with ion Coulomb crystals in an optical cavity, Nat. Phys. **5**, 494 (2009).

[42] H. Maier-Flaig, M. Harder, S. Klingler, Z. Qiu, E. Saitoh, M. Weiler, S. Geprägs, R. Gross, S. T. B. Goennenwein, and H. Huebl, Tunable magnon-photon coupling in a compensating ferrimagnet - from weak to strong coupling, Appl. Phys. Lett. **110**, 132401 (2017).

[43] S. Seki, S. Ishiwata, and Y. Tokura, Magnetoelectric nature of skyrmions in a chiral magnetic insulator Cu_2OSeO_3, Phys. Rev. B **86**, 060403(R) (2012).

[44] J. S. White, K. Prša, P. Huang, A. A. Omrani, I. Živković, M. Bartkowiak, H. Berger, A. Magrez, J. L. Gavilano, G. Nagy, J. Zang, and H. M. Rønnow, Electric-Field-Induced Skyrmion Distortion and Giant Lattice Rotation in the Magnetoelectric Insulator Cu_2OSeO_3, Phys. Rev. Lett. **113**, 107203 (2014).

[45] Y. Okamura, F. Kagawa, S. Seki, and Y. Tokura, Transition to and from the skyrmion lattice phase by electric fields in a magnetoelectric compound, Nat. Commun. **7**, 12669 (2016).

[46] S. P. Wolski, D. Lachance-Quirion, Y. Tabuchi, S. Kono, A. Noguchi, K. Usami, and Y. Nakamura, Dissipation-Based Quantum Sensing of Magnons with a Superconducting Qubit, Phys. Rev. Lett. **125**, 117701 (2020).

[47] A. Chacon, L. Heinen, M. Halder, A. Bauer, W. Simeth, S. Mühlbauer, H. Berger, M. Garst, A. Rosch, and C. Pfleiderer, Observation of two independent skyrmion phases in a chiral magnetic material, Nat. Phys. **14**, 936 (2018).

[48] L. J. Bannenberg, H. Wilhelm, R. Cubitt, A. Labh, M. P. Schmidt, E. Lelièvre-Berna, C. Pappas, M. Mostovoy, and A. O. Leonov, Multiple low-temperature skyrmionic states in a bulk chiral magnet, npj Quantum Mater. **4**, 11 (2019).

[49] S. Khan, O. Lee, T. Dion, C. W. Zollitsch, S. Seki, Y. Tokura, J. D. Breeze, and H. Kurebayashi, Coupling microwave photons to topological spin-textures in Cu_2OSeO_3, Phys. Rev. B **104**, L100402 (2021).

[50] E. Ruff, P. Lunkenheimer, A. Loidl, H. Berger, and S. Krohns, Magnetoelectric effects in the skyrmion host material Cu_2OSeO_3, Sci. Rep. **5**, 15025 (2015).

[51] S. S. Kalarickal, P. Krivosik, M. Wu, C. E. Patton, M. L. Schneider, P. Kabos, T. J. Silva, and J. P. Nibarger, Ferromagnetic resonance linewidth in metallic thin films: Comparison of measurement methods, J. Appl. Phys. **99**, 093909 (2006).

[52] I. Neudecker, G. Woltersdorf, B. Heinrich, T. Okuno, G. Gubbiotti, and C. Back, Comparison of frequency, field, and time domain ferromagnetic resonance methods, J. Magn. Magn. Mater. **307**, 148 (2006).

[53] H. Maier-Flaig, S. T. B. Goennenwein, R. Ohshima, M. Shiraishi, R. Gross, H. Huebl, and M. Weiler, Note: Derivative divide, a method for the analysis of broadband ferromagnetic resonance in the frequency domain, Rev. Sci. Instrum. **89**, 076101 (2018).

[54] S. Klingler, V. Amin, S. Geprägs, K. Ganzhorn, H. Maier-Flaig, M. Althammer, H. Huebl, R. Gross, R. D. McMichael, M. D. Stiles, S. T. B. Goennenwein, and M. Weiler, Spin-Torque Excitation of Perpendicular Standing Spin Waves in Coupled YIG/Co Heterostructures, Phys. Rev. Lett. **120**, 127201 (2018).